

Large-Scale Distribution of Herbig-Haro Objects in Taurus*

Ke-Feng Sun^{1,2,3}, Ji Yang^{3,4}, Shao-Guang Luo^{1,2}, Min Wang^{3,4}, Li-Cai Deng^{2,4},
Xu Zhou^{2,4} and Jian-Sheng Chen^{2,4}

¹ Department of Astronomy, Peking University, Beijing 100871; sunkf@water.pku.edu.cn

² Chinese Academy of Sciences-Peking University Joint Beijing Astrophysical Center, Beijing 100871

³ Purple Mountain Observatory, Chinese Academy of Sciences, Nanjing 210008

⁴ National Astronomical Observatories, Chinese Academy of Sciences, Beijing 100012

Received 2003 March 16; accepted 2003 June 6

Abstract We report our new results on Herbig-Haro (HH) objects in the star forming region of Taurus from a wide-field survey with the 60/90 cm Schmidt telescope of the Beijing Astronomical Observatory. This survey using CCD imaging with a narrow band [SII] filter and an intermediate band [BATC10] filter covered approximately 30 square degrees in Taurus. Besides confirming the known HH Objects in the region, we discovered seven new HH candidates, and groups. Six of these are HH 701A-B, HH 702A-D, HH 703, HH 704A-D, HH 705, HH 706 and the seventh is a group, a new component of HH 319, labeled HH 319B-D. Based on the large-scale distribution of pre-main-sequence (PMS) stars in Taurus, we analyze statistically the most probable distance from the HH objects to each PMS star, from which we estimate the typical timescale of these HH objects to be between $(1.3 - 2.0) \times 10^4$ yrs; and we also obtain the birth rates of HH objects: 0.447 ± 0.198 for Class I PMS stars, 0.360 ± 0.222 for Class II PMS stars, and -0.148 ± 0.234 for Class III PMS stars.

Key words: ISM: Herbig-Haro objects — ISM: individual (Taurus region) — ISM: jets and outflows — star: formation — stars: pre-main-sequence

1 INTRODUCTION

Herbig-Haro (HH) objects are shock-excited nebulae intimately associated with star-formation regions (Schwartz 1978) and are good tracers of the mass outflow activity of young stellar objects (YSOs) (Reipurth & Heathcote 1997). Taurus is one of the nearest active, low-mass star formation regions with more than 80 T Tauri stars identified in infrared and/or optical observations (Cohen & Kuhl 1979; Herbig & Bell 1988; Strom et al. 1989; Kenyon et al. 1990) and about 23 molecular outflows (Wu et al. 2003, in preparation).

* Supported by the National Natural Science Foundation of China.

There are 32 known HH objects in Taurus (Reipurth 1999). Several HH surveys in Taurus have been carried out. Alten et al. (1997) found HH 360–362; Gomez et al. found HH 390–395 ($10' \times 10'$) in 1997; Devine et al. (1999) discovered HH 410–414 toward Haro 6–10 ($H\alpha$ $1^\circ \times 1^\circ$), S[II] $36' \times 36'$) and HH 466–468 were found by Aspin & Reipurth (2000) toward GK Tau region ($6.5' \times 6.5'$). All of the surveys were confined within 1 square degree or less. In this paper, we present the results of our newly- completed HH survey in Taurus, which covered almost 30 square degrees. We also present our statistical results of the most probable distance from the HH objects to the PMS stars and the birth rate of HH objects in Taurus.

2 OBSERVATIONS

The observations were carried out using the 60/90 cm Schmidt telescope at the Xinglong Observatory, Beijing Astronomical Observatory. The telescope is equipped with a thick Ford 2048 \times 2048 CCD at the prime focus of $f/3$. The field of view of this CCD is $58' \times 58'$ and the pixel size is $15\mu\text{m}$, equivalent to $1.71''$ pixel $^{-1}$ (Chen 1994; Fan et al. 1996). A narrowband [SII] filter and a BATC intermediate-band filter [BATC10] were used in our survey. The [SII] filter is centered at 6725\AA with a passband of 50\AA , which covers well the strong and characteristic lines of HH objects ([S II] $\lambda\lambda 6717/6731$). The [BATC10] filter is centered at 7050\AA with a bandwidth of 300\AA , which covers no characteristic lines of HH objects and thus was used to measure the continuum.

We obtained the [SII] and continuum images from 2001 December to 2002 January. Three frames in each band were taken so that cosmic rays and bad pixels may be removed. The total exposure time was 3600 s in the [SII] band and 900 s in the [BATC10] band. The survey region of Taurus was divided into 30 target fields, which covered most of the Taurus dark molecular cloud region.

The seeing during the observations was typically $\sim 2''$ and our detecting limit was between 19.5^{m} and 20.6^{m} . Bias subtraction, dome flat-field normalization, and image combination were made using the IRAF package. All the data obtained in this survey were processed through the same pipeline programs as those in our previous works (Zhao et al. 1999; Wang et al. 2000; Wu et al. 2002). The detailed technical description of the pipeline scheme was given in Deng et al. (2001).

3 RESULTS AND DISCUSSION

As a result of the survey, we have discovered six new HH objects and several new components of HH 319 (Table 1). Of the seven new HH objects, four are groups of individuals. We have also confirmed the 22 known HH objects presented in Reipurth (1999). Against the total number of known HH objects in this region, the detection rate of our survey is about 70%. The S[II] images of all the newly discovered HH objects are displayed in Fig. 1.

HH 701 is an isolated HH group, composed of two parts with the southern one being fainter. No infrared source was found around it and there is neither outflow or known HH object nearby. HH 702 is divided into four parts which are numbered as A to D from north-east to southwest. These four parts are all very faint knots. There are three IRAS sources nearby. IRAS 04234+2547 is located $4.34'$ to the southeast to HH 702A; IRAS 04237+2559 and IRAS 04236+2559 are, respectively, located in the northwest and are $8.55'$ and $8.79'$ away. Two HH objects, HH 159 and HH 158, are located $9.78'$ and $10.60'$ to the northwest of HH 702A.

Table 1 Newly Discovered Herbig-Haro Objects in Taurus

Name	$\alpha(2000)$	$\delta(2000)$	Comments
HH 701A	04:12:16.44	28:50:15.0	Knot
HH 701B	04:12:17.99	28:49:31.7	Faint Knot
HH 702A	04:26:35.65	25:57:54.7	Faint Knot
HH 702B	04:26:34.32	25:57:39.7	Faint Knot
HH 702C	04:26:34.10	25:57:40.3	Faint Knot
HH 702D	04:26:34.11	25:57:23.2	Faint Nebula
HH 319A	04:32:39.38	24:21:25.8	Former HH 319
HH 319B	04:32:38.81	24:20:55.4	Knot
HH 319C	04:32:36.63	24:20:29.8	Faint Knot
HH 319D	04:32:31.75	24:20:03.1	Faint Knot
HH 703	04:35:01.89	23:38:58.4	Nebula
HH 704A	04:38:45.09	25:18:14.3	Knot
HH 704B	04:38:46.21	25:18:04.8	Bright Knot
HH 704C	04:38:50.60	25:18:17.4	Knot
HH 704D	04:38:52.49	25:18:17.3	Nebula
HH 705	04:39:06.72	26:20:29.9	Nebula
HH 706	04:39:11.44	25:27:19.0	Fuzzy Nebula

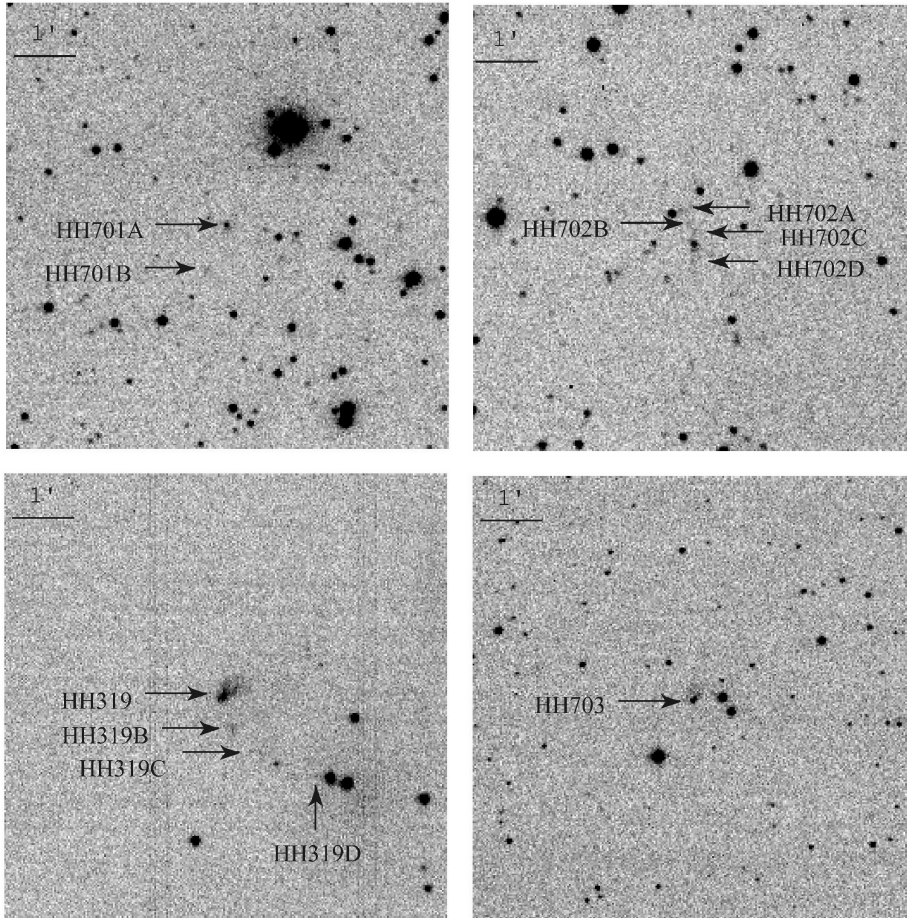


Fig. 1 [S II] images of the newly discovered HH objects in Taurus. North is up and east is left.

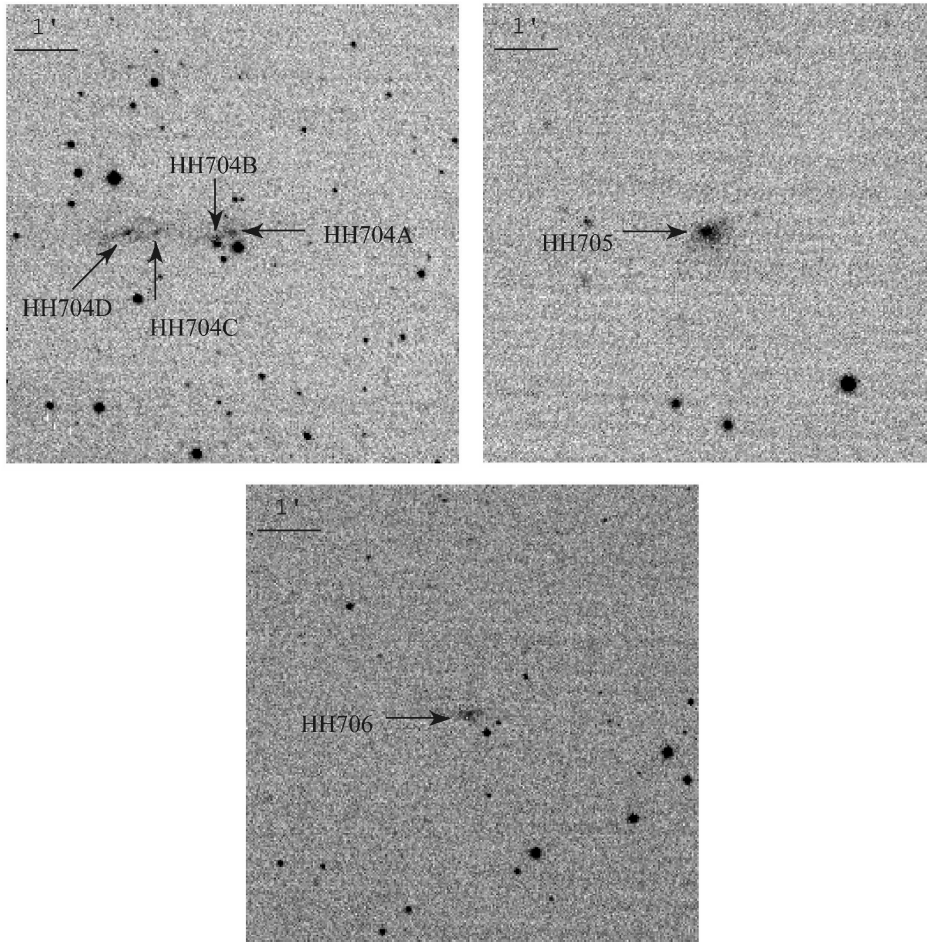


Fig.1 Continued.

From one of the known HH objects, HH 319, we found three additional HH components, HH 319B-D. Among them, HH 319B and HH 319D were also discovered by Magakian et al. (2002) and labeled as object 1 and object 2 there. HH 319C is a faint object and needs further observation to confirm its nature.

HH 703 is a nebulous object and no infrared or radio source was detected within $10'$. HH 704 is an HH group of four parts, it extends $\sim 2'$ along the declination direction. HH 704A-C are all knots and HH 704B is the brightest one, while HH 704D appears as a bright nebula. IRAS 04356+2516 is the only infrared source nearby, and it is $4.31'$ northeast of HH 704A.

HH 705 appears as a nebula. Two radio sources, LDN 1527 1 and LDN 1527 2, are located $3.65'$ southeast and $5.00'$ southwest to HH 705. There are also two YSOs, ITG 11 and ITG 14, which are located $7.88'$ and $9.98'$ to the southwest of HH 705, respectively. HH 706 looks like a fuzzy nebula. There are four infrared sources within $10'$. ITG 9, ITG 9B and ITG 9C are located $6.38'$, $6.41'$ and $6.53'$ to the southwest of HH 706, respectively, and IRAS 04356+2516

is $7.75'$ southeast of HH 706. IRAS 04357+2528 is located $8.28'$ to the southwest of HH 706.

Figure 2 shows the large-scale spatial distribution of our HH objects, along with the known HH objects and the CO outflows selected from the most recent outflow catalog (Wu et al. 2003). In the same figure, we have superimposed the distribution of dense molecular gas as given by the ^{13}CO contour map (Mizuno et al. 1995). Within the scope of survey, the HH objects exhibit a general accordance with the large-scale CO distribution.

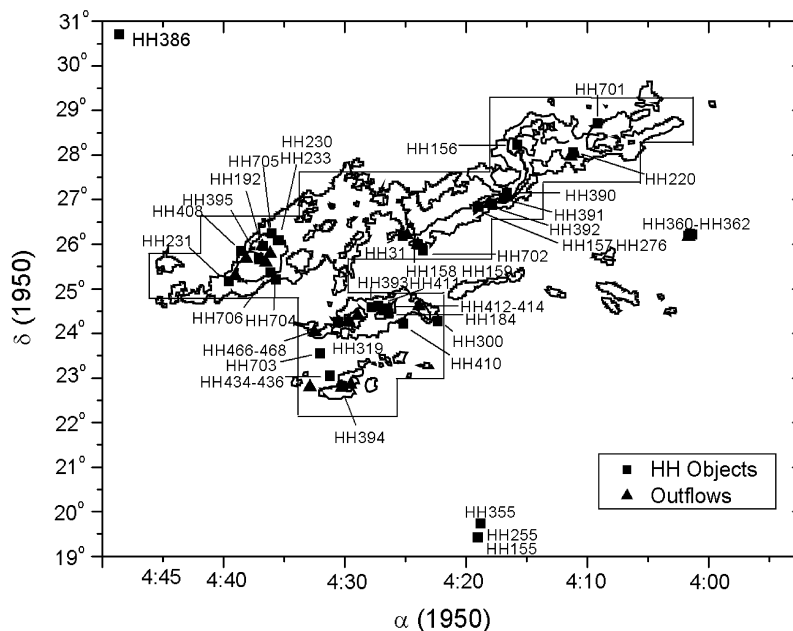


Fig. 2 Positions of the all HH objects and the CO outflows. The superposed contours are the $^{13}\text{CO} J = 1 - 0$ brightness distribution from Mizuno et al. (1995). The region delimited by the straight lines is our survey area, which is 30 deg^2 and covers almost the whole Taurus region. The distribution of the HH objects accords with the CO emission distribution: most of them located in the dense parts while some have moved out of the CO emission.

From Fig. 2, we can identify some clustered structure in the spatial distribution of these HH objects. The newly discovered HH objects are mostly close to previously known HH objects and form five primary groups. Only a few HH objects such as HH 156, HH 220 and HH 701 are found away from the groups, showing that star formation is more active in the five groups. From the same figure, we can also see that most of the HH objects, especially those in groups, are well associated with molecular outflows, which is in accordance with the physical nature of the HH objects.

To understand the relationship between HH objects and pre-main-sequence stars more clearly, we used the data of our newly-found HH objects, of the previously known HH objects and of the known PMS stars in Taurus (Kenyon & Hartmann 1995; Hartmann 2002) to seek statistical relationship between them.

First, we plotted the positions and map of the new and known known HH objects, the CO outflows and the PMS stars (Fig. 3). From Fig. 3, we can see that the distributions of the HH objects, the outflows and the PMS stars are concentrated in the same localities, indicating the

close relationship between the HH objects and the PMS stars. A more detailed discussion now follows.

In a crowded HH region such as the Taurus, it is hard to trace each HH object back to its driving source. Instead, the statistical distance between HH objects and their nearby young stellar objects will provide an effective estimate of typical scale of HH excitation. We calculate the distance of every HH object to every PMS star to find the most probable distance between the HH objects and the PMS stars. We divided the PMS stars into three classes, labeled I, II, III, according to their spectral energy distribution. The statistics includes 38 HH objects (32 known HH objects plus 6 new HH objects), 21 Class I stars, 76 class II stars and 31 class III stars.

For class I stars, the number of pairs is 798 (21×38); for class II stars, the number is 2888 (76×38); for class III stars, the number is 1178 (31×38); for all the PMS stars, the number is 4864. After the computation, we cumulate the distances into one pc bins. Then we fit the results with a Gaussian function:

$$y = y_0 + \frac{A}{w \cdot \sqrt{\frac{\pi}{2}}} e^{-\frac{2(x-x_0)^2}{w^2}}. \quad (1)$$

The parameters of the Gaussian fit are listed in Table 2 and the result is presented in Fig. 4.

From Table 2, we obtain that the mean distances from HH objects to the class I, II, and III PMS stars are, respectively, 5.50, 6.18, and 6.76 pc. It means that HH objects are closest to class I PMS stars, then to class II PMS stars and least close to class III PMS stars. This is consistent with the picture that HH objects are moving away from young stellar objects with increasing stellar ages. From our results, one can estimate that HH objects have a closer relationship with class I than with class II PMS stars. Assuming typical proper velocity of the HH objects to be a few hundred km s^{-1} (here we assumed 400 km s^{-1}), we evaluate that typical timescale of these HH objects is between $(1.3 - 2.0) \times 10^4$ yrs (Table 2).

Table 2 Statistical Parameters of Gaussian Fit for the Distances between the HH Objects and the PMS Stars in Taurus

	w	x_0 (pc)	t_0 (yr)	x_1 (pc)	t_1 (yr)
Class I stars	9.90	5.50	1.3×10^4	6.66	1.6×10^4
Class II stars	14.23	6.18	1.5×10^4	7.75	1.9×10^4
Class III stars	15.80	6.76	1.7×10^4	8.00	2.0×10^4

Note: w : 2σ , approximately 0.849 the width of the peak at half height; x_0 : the center value ($w/2$ is the standard deviation while x_0 denotes mean value); t_0 : the timescale from mean distance; x_1 : the weight distance; t_1 : the timescale from weight distance.

Using the survey results, we calculate the birth rate of HH objects in Taurus. After trying different area size, we find that the $1^\circ \times 1^\circ$ size was the best one which has nothing to do with our division of the observation areas. So we divide the Taurus area into 30 sub areas of this size. For each area, we count the numbers of HH objects and of PMS stars. We examine the birth rate with class I stars, class II stars and class III stars. We obtain respectively 19, 29, and 24 pairs of data for class I, II, III stars. The results are presented in Fig. 5. Then we make least squares linear fits $y = A + Bx$ to the points. The parameters from the fitting are listed in Table 3 and the fitting is displayed in Fig. 5.

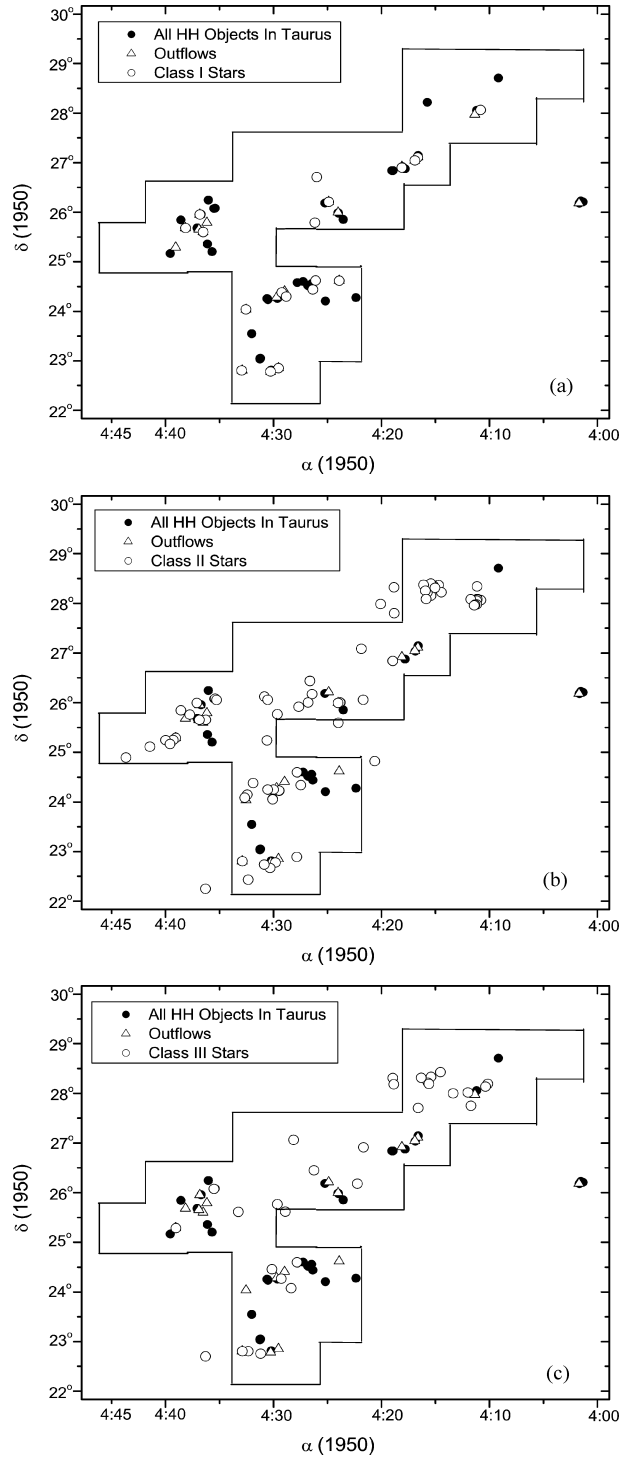


Fig. 3 Map and positions of the all HH objects, the CO outflows and the PMS stars. The region delimited by the straight lines is our survey area. In Fig. 3(a), the PMS stars are exclusively class I stars; In Fig. 3(b), exclusively class II stars; In Fig. 3(c), exclusively class III stars.

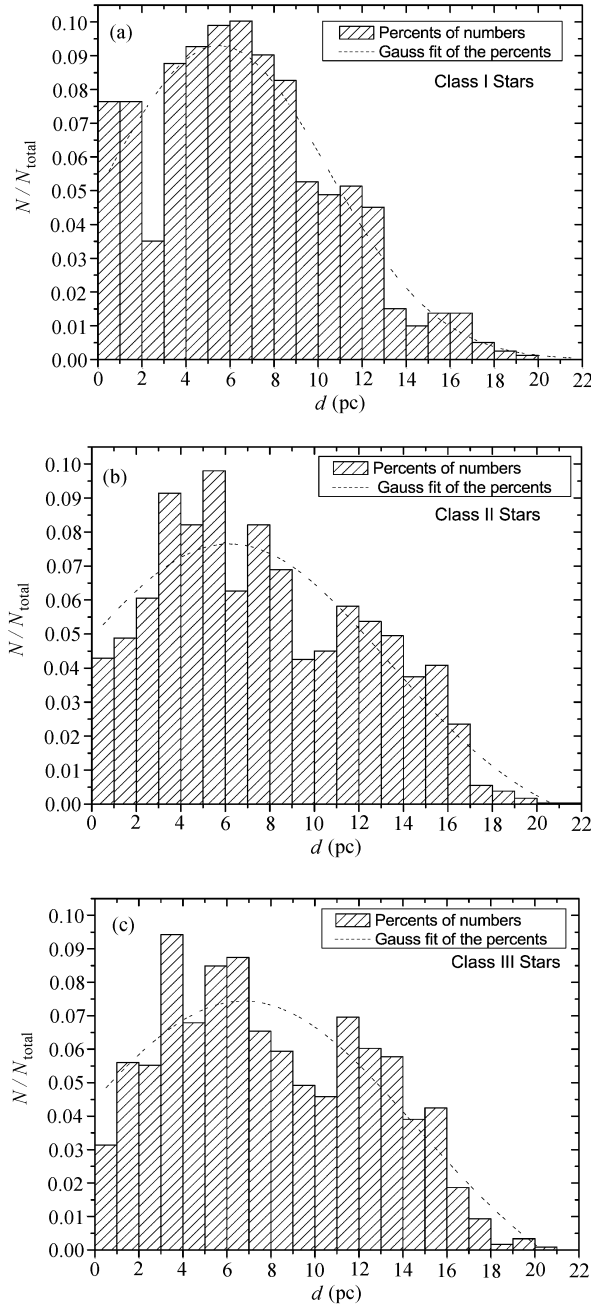


Fig. 4 Probability of the distance between the HH objects and the PMS stars in Taurus. The Y-coordinate is the probability of the HH objects within one pc (the fraction of the total number of HH objects in the given distance bin). The X-coordinate is the distance from the HH objects to the PMS star of class I (a), of class II (b) and of class III (c).

Table 3 Statistical Parameters of Linear Fit for the Birth Rate of HH Objects in Taurus

	N	A	B	R	SD	P
Class I stars & HH objects	19	0.029±0.014	0.447±0.198	0.48	0.042	0.04
Class II stars& HH objects	29	0.022±0.011	0.360±0.222	0.30	0.044	0.12
Class III stars& HH objects	24	0.048±0.014	-0.148±0.234	- 0.13	0.047	0.53

Note: The confidence level in the linear fits is 95%. N: number of data points; A: intercept value and its standard error; B: slope value and its standard error (value of birth rate of HH objects); R: correlation coefficient; SD: standard deviation of the fit; P: the null probability (that R is zero).

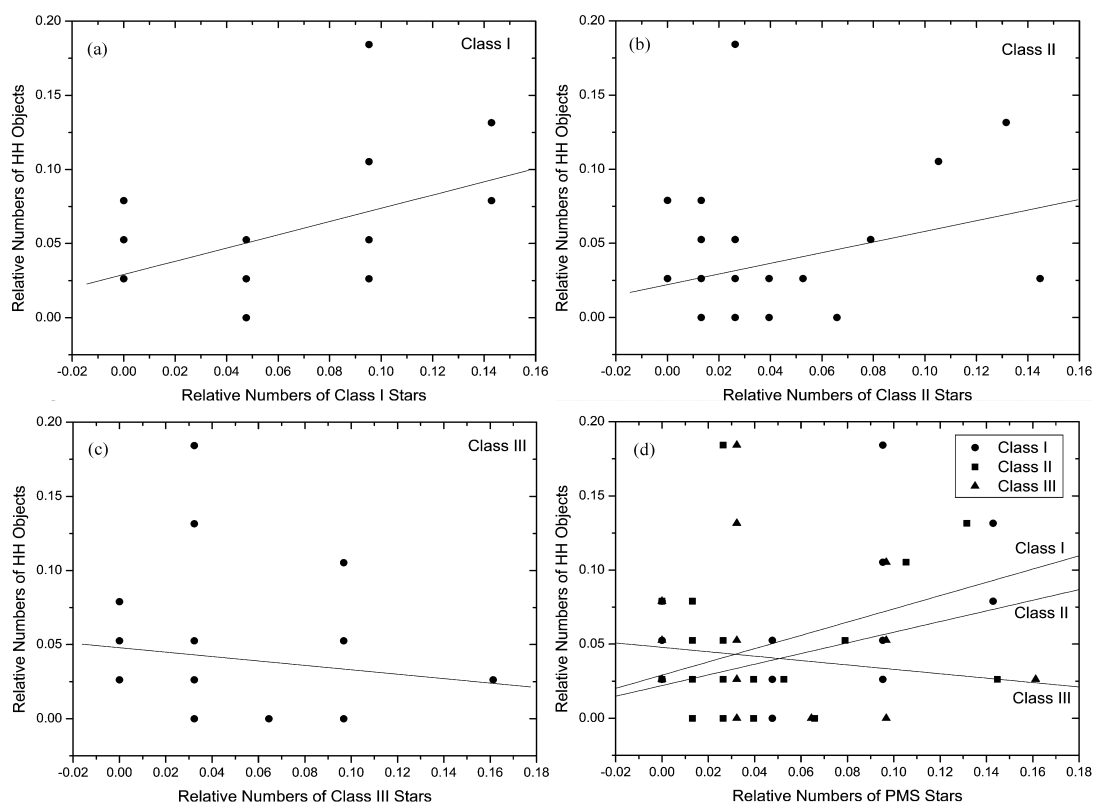


Fig. 5 Birth rate of HH objects in Taurus. The Y-coordinate is the relative numbers of HH objects in a $1^\circ \times 1^\circ$ region and the X-coordinate is the relative numbers of PMS stars in the same region of class I (a), of class II (b); of class III (c) and of all three classes (d).

From the distribution of the points, the fitted lines and Table 3, we can see that there is a positive correlation between the HH objects and the PMS stars. For the class I PMS stars, the correlation is the best; for the class II PMS stars, the correlation is still positive but is not as significant as for the class I stars. For the class III PMS stars the correlation is vague or even negative, which means that as the number of class III PMS stars increases in a region, the

number of HH objects in that region actually decreases. Moreover, we can also estimate the birth rates of the HH objects, which are 0.447 ± 0.198 for Class I PMS stars, 0.360 ± 0.222 for Class II PMS stars and -0.148 ± 0.234 for Class III PMS stars (Table 3).

As we know, most of HH objects are produced in the early stage of star formation and they are short-lived objects. It is reasonable that the number of HH objects should increase with increasing numbers of class I or class II PMS stars in the same region. From our statistics, we can estimate that those PMS stars in the stage of class I excite more HH objects than those in the stage of class II. The decreasing number of HH objects with class III PMS stars indicates that previously excited HH objects are beginning to decay at the longer timescale. The number of HH objects is approximately balanced at a timescale comparable to that of class II objects. For further information and detailed studies, it will be instructive to compare our results in Taurus with the results in other nearby star formation regions, such as Orion, Ophiuchus, etc.

4 CONCLUSIONS

Six new HH objects and new components of HH 319 were discovered in this survey, and three of the new HH objects are in groups.

The most probable distance from HH objects to PMS stars in Taurus has been obtained statistically, ranging from 5.50 pc to 6.76 pc for class I-III stars. The timescale of HH objects is from $(1.3 - 2.0) \times 10^4$ yrs.

The birth rates of HH objects in Taurus have also been obtained in this survey: 0.447 ± 0.198 for class I PMS stars, 0.360 ± 0.222 for class II PMS stars and -0.148 ± 0.234 for class III PMS stars. The HH objects have the closest relation with the class I PMS stars, while the correlation of HH objects with class III PMS stars is negative. The number of HH objects is approximately balanced at a timescale comparable with the age of class II PMS stars, which is slightly longer than the timescale we obtained from the mean distance between the HH objects and the PMS stars in Taurus.

Acknowledgements We specially thank the staff members of the BATC Beijing group for their excellent support during the observations. We appreciate valuable discussions with J. W. Wu, H. C. Wang, C. B. Jiang. This work was supported by NSFC grant 10133020 and the Ministry of Science and Technology of China through grant G1990754.

References

- Alten V. P., Bally J., Devine D., Miller G. J., 1997, IAUS, 182, 51
- Aspin C., Reipurth B., 2000, MNRAS, 311, 522
- Chen J., 1994, In: IAU Symp. 161, Astronomy from Wide-Field Imaging, H. T. MacGillivray, E. B. Thomson, B. M. Lasker, I. N. Reid, D. F. Malin et al. eds., Dordrecht: Kluwer, 17
- Cohen M., Kuhl L. V., 1979, ApJ, 307, 337
- Deng L., Yang J., Zheng Z., Jiang Z., 2001, PASP, 113, 463
- Devine D., Reipurth B., Bally J., Balonek T. J., 1999, AJ, 117, 2931
- Fan X., Burstein D., Chen J.-S., Zhu J., Jiang Z. et al., 1996, AJ, 112, 628
- Gomez M., Kenyon S. J., Whitney B. A., 1997, AJ, 114, 265
- Herbig G. H., Bell K. R., 1988, Third Catalog of Emission-Line Stars of the Orion Population, Lick Obs. Bull., No. 1111, University of California
- Hartmann L., 2002, ApJ, 578, 914

- Kenyon S. J., Hartmann L., 1995, *ApJS*, 101, 117
- Kenyon S. J., Hartmann L. W., Strom K. M., Strom S. E., 1990, *AJ*, 99, 868
- Magakian T. Yu., Movsessian T. A., Ogura K., Afanasiev V. L., 2002, *A&A*, 383, 598
- Mizuno A., Onishi T., Yonekura Y., Nagahama T., Ogawa H., Fukui Y., 1995, *ApJ*, 445, L161
- Reipurth B., 1999, *A General Catalogue of Herbig-Haro Objects*, 2 Edition, <http://casa.colorado.edu/hhcat>
- Reipurth B., Heathcote S., 1997, In: *IAU Symp. 182, Herbig-Haro Flows and the birth of Low Mass Stars*, B. Reipurth, C. Bertout, eds., Dordrecht: Kluwer, 3
- Schwartz R. D., 1978, *ApJ*, 223, 884
- Strom K. M., Strom S. E., Edwards S., Cabrit S., Skrutskie M. F., 1989, *AJ*, 97, 1451
- Wang M., Zhao B., Yang J., Deng L., Chen J., 2000, *Chinese Phys. Lett.*, 17, 304
- Wu J., Wang M., Yang J., Deng L., Chen J., 2002, *AJ*, 123, 1986
- Wu J., Wu Y., Wang J., Cai K., 2002, *Chin. J. Astron. Astrophys.*, 2(1), 33
- Wu Y. et al., 2003, in preparation.
- Zhao B., Wang M., Yang J., Wang H., Deng L., Yan J., Chen J., 1999, *AJ*, 118, 1347